Analytical Methods

International Edition: DOI: 10.1002/anie.201708958
German Edition: DOI: 10.1002/ange.201708958

A Peroxisome-Inspired Chemiluminescent Silica Nanodevice for the Intracellular Detection of Biomarkers and Its Application to Insulin-Sensitizer Screening

Xu Jie, Haimei Yang, Min Wang, Yue Zhang, Weili Wei, and Zhining Xia*

Abstract: *The profiling of oxidase-catalyzed biomarkers is an essential procedure for the diagnosis and precise treatment of metabolic diseases. Inspired by the metabolism of H_2O_2 in peroxisomes, a novel chemiluminescent silica nanodevice (CSN) was designed for the sensitive and selective sensing of intracellular oxidase-catalyzed biomarkers. Oxidases catalyzed the oxidation of biomarkers followed by the production of H_2O_2, and then the generated H_2O_2 was employed to trigger chemiluminescence of the CSN. Utilizing this nanodevice, we not only accurately quantified intracellular glucose but also developed its further application for facile insulin sensitizer screening. Furthermore, sensitive and multiparametric analysis of oxidase-catalyzed biomarkers like lactic acid, uric acid, and ethanol was demonstrated. Thus, this peroxisome-inspired CSN holds great promise for the general diagnosis of metabolic diseases and in drug discovery.*

Oxidases are involved in the H_2O_2-generating catabolism of numerous biomarkers such as D-glucose, L-lactic acid, uric acid, ethanol, cholesterol, and fatty acids. The abnormal catabolism of these biomarkers is closely related to various metabolic diseases including diabetes, lactic acidosis, gout, and obesity.[1] Therefore, the monitoring of these related biomarkers is routinely required for disease diagnosis, to understand pathogenic processes, and to evaluate pharmacologic responses to a therapeutic intervention. Traditional chromatographic, spectrometric, and electrochemical methods have been widely used for the off-line quantitative analysis of these biomarkers.[2] However, these methods suffer from low specificity, tedious procedures, or requirement of bulky equipment and highly skilled operators. Moreover, they lack the ability to detect intracellular biomarkers in a non-invasive way and thus cannot provide the real-time and spatial distribution of biomarkers at the cellular level. Recently, many fluorescence-based biosensors for the non-invasive analysis of the aforementioned small-molecule biomarkers have been developed.[3] For instance, a fluorescent probe was developed for the imaging of glucose uptake in living cells.[4] They are effective but usually showed several disadvantages such as the requirement of a bulky excitation light source, strong background interference from biological matrices, and low robustness owing to photobleaching of the probes.[5]

Chemiluminescence (CL) has attracted extensive attention in recent decades because of its high sensitivity, accurate quantification, simple instrumentation, and lack of photoexcitation requirement.[6] Until now, various H_2O_2-mediated CL systems based on luminol, lucigenin, or peroxyoxalate (PO) were developed.[7] Among them, the PO-CL system was broadly used in consumer products such as light sticks and fishing lures and in biological diagnosis because of its high CL efficiency, durable lifetime, and tunable CL wavelength.[8] Additionally, the PO-CL system has a highly sensitive and selective response toward H_2O_2[9] and thus has potential applications in the detection of biomarkers that can produce H_2O_2 catalyzed by oxidases. However, most PO-CL reagents are hydrophobic and thus cannot be readily applied to aqueous bio-systems.[10] Hence, it is challenging to develop a hydrophilic PO-based CL probe for in situ or even intracellular H_2O_2 detection. In this regard, one pioneering work has shown the successful design of a novel CL probe for in vivo imaging of H_2O_2 in the peritoneal cavity of living mice by using oxalate-grafted polymeric nanoparticles.[11] Nevertheless, the authors did not illustrate the intracellular detection of H_2O_2. Polymeric nanoparticles with diameters larger than 150 nm would be mostly excluded from cellular internalization by non-phagocytic cells.[12] Thus the nanoparticles[11] may preclude the capability of intracellular detection due in part to their larger size (ca. 550 nm). Moreover, their CL quantum yield (CL-QY) can be further improved by substituting a phenyl moiety with electron-withdrawing groups.[9,13] The use of highly efficient PO-CL reagents has been carried by loading PO-CL reagents in hydrophobic micro-containers such as micelles.[14] However, those strategies were not used to detect intracellular H_2O_2, much less H_2O_2-generating biomarkers.

Interestingly, in virtually all eukaryotic cells, the oxidase-catalyzed H_2O_2-generating bioreactions and subsequent scavenging of H_2O_2 for avoiding its toxicity are mainly carried in the organelle peroxisomes (Scheme 1 a).[15] Inspired by the two-step metabolism of H_2O_2 generation and scavenging within peroxisomes, we proposed a new strategy for the general intracellular detection of oxidase-catalyzed biomarkers by employing the released H_2O_2 as the messenger and a high QY PO-CL probe as the sensitive and selective reporter for H_2O_2 (Scheme 1 b). As a demonstration, a novel chemiluminescent silica nanodevice (CSN) was constructed for both disease diagnosis (that is, in situ and intracellular detection of oxidase-catalyzed biomarkers) and drug devel-

[*] Dr. X. Jie, H. Yang, M. Wang, Y. Zhang, Prof. W. Wei, Z. Xia
School of Pharmaceutical Sciences and Innovative Drug Research Centre, Chongqing University
Chongqing 401331 (P. R. China)
E-mail: wlwei@cqu.edu.cn

Supporting information and the ORCID identification number(s) for the author(s) of this article can be found under: https://doi.org/10.1002/anie.201708958.

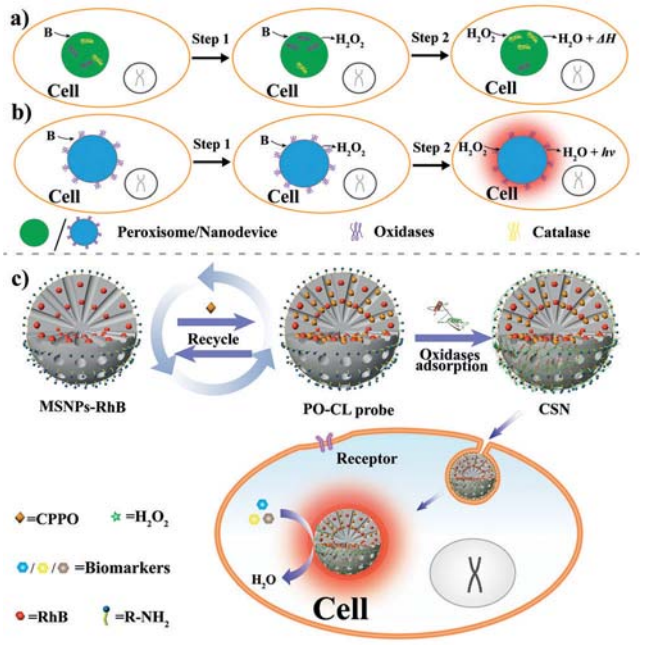

Scheme 1. The two-step process of a) H_2O_2 generation and scavenging in the peroxisome and b) the peroxisome-like chemiluminescent nanodevice. c) The fabrication process of the CSN and its application in intracellular oxidase-catalyzed biomarker detection. ΔH = enthalpy change.

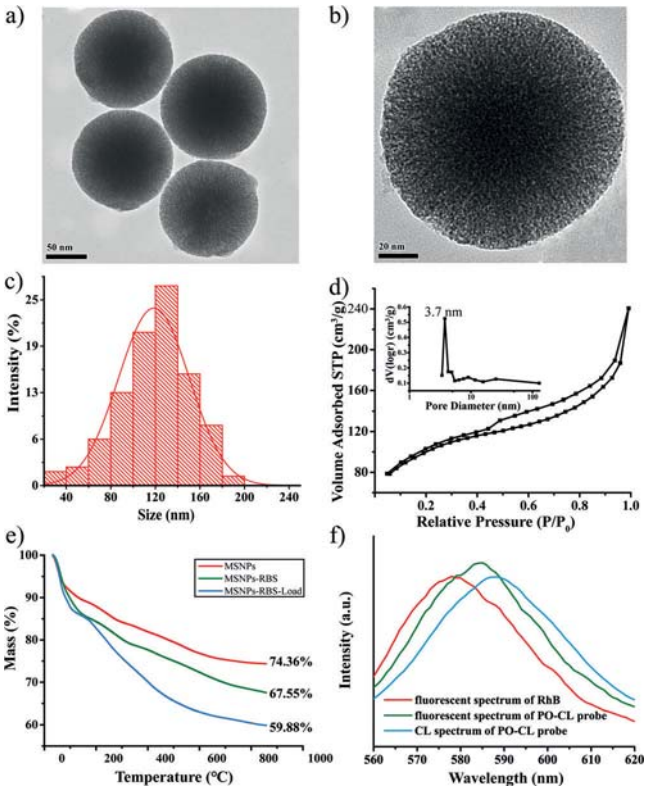

Figure 1. a,b) Representative TEM and HRTEM images of MSNPs-RhB. c) Size distribution of MSNPs-RhB (152 samples). d) N_2 adsorption–desorption isotherms and pore-size distribution curves (inset) of MSNPs-RhB. e) TGA curves with the heating rate of 10 °C min^{-1}. f) Fluorescence spectra of RhB and PO-CL probe and the CL spectrum of PO-CL probe, which was stimulated with H_2O_2. [RhB] = 10 μM, [PO-CL probe] = 500 μg mL^{-1}, [H_2O_2] = 100 μM, 20 mM PBS (pH 7.2) as solvent, λ_{ex} = 555 nm, 25 °C.

opment (that is, insulin sensitizer screening). As shown in Scheme 1 c, the CSN contains three essential components: 1) Biocompatible mesoporous silica nanoparticles for the storage and delivery of highly H_2O_2-sensitive bis(2-carbopentyloxy-3,5,6-trichlorophenyl) oxalate (CPPO), 2) rhodamine B (RhB) covalently doped in the silica skeleton as the fluorescent reporter for converting chemical energy into a light signal, and 3) the electrostatically adsorbed oxidases on the surface of mesoporous silica as the converter for selectively catalyzing the oxidation of biomarkers to produce the messenger molecule H_2O_2. It is noteworthy that the adsorbed oxidases not only could remain active as previously reported,[16] they also formed a compact shell to protect CPPO from leaking. In this paper, we first characterized the CSN; then, the luminescence properties such as dynamics and stability were investigated. Subsequently, a series of biomarkers including glucose, alcohol, lactic acid, and uric acid were used to verify the ability of the CSN to detect the oxidase-catalyzed biomarkers for disease diagnosis. To demonstrate its potential application in drug development, the model drug insulin sensitizers for diabetic therapy were also screened by the glucose oxidase-adsorbed CSN.

To construct the intelligent CSNs, covalently RhB-doped mesoporous silica nanoparticles (MSNPs-RhB) were first prepared according to a modified sol-gel method (see the Supporting Information).[17] TEM (Figure 1 a) and high-resolution TEM (HRTEM, Figure 1 b) images showed the spherically shaped MSNPs-RhB with an ordered mesoporous structure and an average diameter of 118 ± 31 nm (Figure 1 c). The mesoporous structure was further confirmed by N_2 adsorption–desorption analysis (Figure 1 d). Pore volume, specific surface area, and pore-size distribution of MSNPs-RhB were 0.233 cm^3 g^{-1}, 350.464 m^2 g^{-1}, and 3.7 nm, respectively. These characteristics endowed MSNPs-RhB with an enormous loading capacity for PO-CL reagents. The FTIR spectrum of MSNPs-RhB showed an emerging band at 1650 cm^{-1} ascribed to the CO–NH stretching vibration (Supporting Information, Figure S1), which suggested the covalent doping of RhB in the MSNPs. The amount of the doped RhB was estimated to be ca. 6.81 wt % by thermogravimetric analysis (Figure 1 e). After loading CPPO into MSNPs-RhB (designated as the PO-CL probe), the characteristic band of CPPO at 1788 cm^{-1} in its FTIR spectrum was observed and ascribed to the vibration of the oxalate group of CPPO, demonstrating the successful loading of CPPO into MSNPs-RhB (Figure S1). Furthermore, by comparing the thermogravimetric curves of MSNPs-RhB and PO-CL probe, the calculated CPPO loading amount was as high as 7.67 % by mass, which allows continuous long-time CL sensing (Figure 1 e). Then, the CL spectrum of the PO-CL probe with stimulation of H_2O_2 was measured. As shown in Figure 1 f, the maximum CL peak of the PO-CL probe was at 588 nm, which was red-shifted 3 and 10 nm with respect to the fluorescent spectra of RhB and PO-CL probe, respectively. The red

luminescence suggested that the probe was suitable for biological analysis.

To validate the feasibility of the PO-CL probe for H_2O_2 sensing, we monitored the CL signals of the PO-CL probe in the presence of different concentrations of H_2O_2 in phosphate buffered saline (PBS). As shown in Figure 2a, the CL half-life

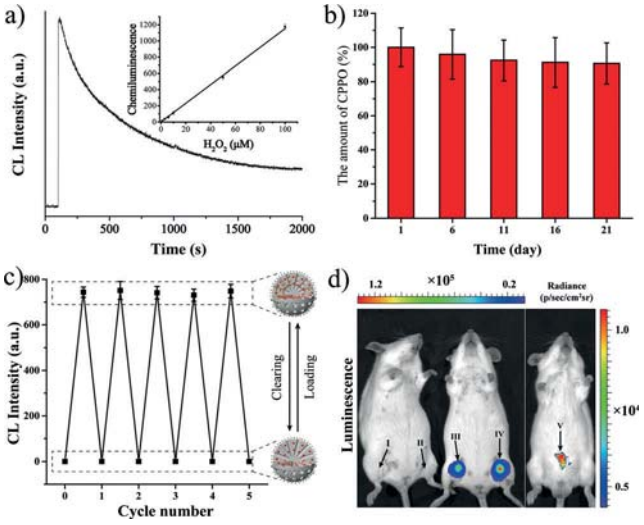

Figure 2. a) CL kinetics curve of PO-CL probe with H_2O_2 stimulation (H_2O_2 was injected at 100 s). Inset: Calibration curve of CL signal response to H_2O_2 concentration. b) Stability of PO-CL probes with added stabilizer and stored at −20 °C. c) Reusability of MSNPs-RhB. d) In vivo imaging of exogenous and endogenous H_2O_2 in mice. I) Negative control, II) PO-CL probe only, III) PO-CL probe + 2 μM H_2O_2, IV) PO-CL probe + 8 μM H_2O_2, and V) LPS (20 μL, 2.5 mg mL^{-1}) + PO-CL probe. Data represent mean ± SD ($n = 3$).

of the PO-CL probe was 3.37 min. Moreover, this assay established a linear dependence ($R^2 = 0.998$) of CL intensity on H_2O_2 concentration from 1.0 to 100.0 μM, indicating that the PO-CL probe incorporating hydrophobic CPPO can be successfully applied to the quantitative detection of H_2O_2 in aqueous systems. In addition, the PO-CL probe retained 90.6% of its initial activity after 21 days of storage in a sealed tube with acetone at −20 °C (Figure 2b), demonstrating the excellent stability of the probe. Due to the covalent doping of RhB to the skeleton of silica, the MSNPs-RhB could be reused. Figure 2c shows that the MSNPs-RhB could be reused for at least five cycles of cleaning and loading of CPPO without significant loss of the CL intensity of the PO-CL probe.

H_2O_2 production is related to oxidative stress and inflammation in aging, injury, and disease.[18] The fast, visual detection of H_2O_2 in vivo is important for disease diagnosis. The constructed PO-CL probe has a long emission wavelength (588 nm) and consequent high level of tissue penetration, suggesting its potential for in vivo imaging of H_2O_2 in deep tissue. To verify this, the in vivo imaging of exogenous H_2O_2 in the thighs of live mice was monitored. As shown in Figure 2d, there was no obvious CL signals for the control group (I) or the PO-CL probe-only group (II). However, a strong CL emission was observed for the mice with co-injection of the PO-CL probe and H_2O_2, a peak emission intensity of 30000 p s^{-1} cm^{-2} sr^{-1} for 2 μM H_2O_2 (III) and 80000 p s^{-1} cm^{-2} sr^{-1} for 8 μM H_2O_2 (IV). The PO-CL probe was also used to image endogenously generated H_2O_2 in vivo. Lipopolysaccharide (LPS) was injected into the peritoneal cavity to induce acute inflammation. Subsequently, PO-CL probes were injected and an obvious CL emission of 8000 p s^{-1} cm^{-2} sr^{-1} was observed as shown in Figure 2d (V).

To detect oxidase-catalyzed biomarkers, oxidase-immobilized CSNs were constructed. Glucose oxidase (GOx), a frequently used specific enzyme for glucose sensing,[19] was electrostatically adsorbed onto the surface of MSNPs-RhB (G-CSN) and its performance on the extra- and intracellular detection of glucose was studied. A visible coating layer on the PO-CL probe was observed in the representative HRTEM image of G-CSN, and the distinct porous channel of the PO-CL probe disappeared because of the shielding of the electron beam by GOx (Supporting Information, Figure S2), which suggested that GOx was successfully deposited. For further confirmation, zeta potential and dynamic light scattering (DLS) analysis were also employed. The zeta potential of the nanodevice changed from $+8.72 \pm 0.85$ to -12.70 ± 0.30 mV and its diameter changed from 125 to 140 nm after GOx coating (Supporting Information, Figure S3). These results further demonstrated that G-CSN was successfully constructed. According to previous reports,[20] hydrophobic molecules in mesoporous silica showed negligible release because of their low solubility. Moreover, because GOx is larger than the pore of the PO-CL probe,[21] the gating of the adsorbed GOx may further avoid the leakage of CPPO in the aqueous environment, but the generated small H_2O_2 molecules can freely transfer into the pores. As expected, a negligible release of CPPO was observed when CPPO-loaded silica nanoparticles were soaked in PBS for 3 h (Supporting Information, Figure S4). The CPPO was stable in PBS over 3 h in the presence of stabilizer (Figure S4c).

Before testing the response of G-CSN to glucose, several factors including the adsorption time of GOx, the CL half-time, and cytotoxicity of G-CSN were studied. The adsorption amounts of oxidase after incubation for 1, 5, 10, and 15 min were similar because of the rapid adsorption of the oxidase onto the surface of silica (Supporting Information, Figure S5). As a compromise between the catalytic activity of GOx and the stability of CPPO in G-CSN, the adsorption time of 5 min was used for the following trials. In addition, the CL kinetics of G-CSN for the glucose response was investigated (Supporting Information, Figure S6). Compared to the direct reaction between the PO-CL probe and H_2O_2, G-CSN exhibited a longer CL half-life of 36.07 min because of the continuous formation of H_2O_2 through the GOx-catalyzed oxidation of glucose and thus provided a long-time signal for sensing. The cytotoxicity of G-CSN was also investigated (Supporting Information, Figure S7), which was negligible in human hepatoma (HepG2) cells even at a concentration as high as 200 μg mL^{-1}. Overall, these results demonstrated that the G-CSN could be an effective probe for both extracellular and intracellular glucose profiling.

The response of G-CSN to different concentrations of glucose in PBS was measured over a range of 2.0–200.0 μM (Supporting Information, Figure S8). The resulting curve showed good linearity ($R^2 = 0.995$). The detection limit (0.47 μM) is much lower than the normal level of intracellular glucose,[22] enabling us to use this G-CSN for intracellular glucose monitoring. To validate the tolerance and accuracy of G-CSN detection in a biological environment, we also used the G-CSN to evaluate the blood glucose levels of live mice. After 12 h of fasting, the blood glucose was monitored at hourly intervals by using both G-CSN and standard glucose testing strips (Supporting Information, Figure S9). The consistency of the blood glucose levels measured using G-CSN and the commercial testing strips demonstrated that the other components in serum did not show significant interference and the G-CSN was reliable even in the complex biological fluids.

The level of intracellular glucose is related to many physiological or pathological conditions such as exogenous glucose level, insulin level, and the receptor sensitivity toward insulin. The low sensitivity of the body to insulin would lead the occurrence of diabetes.[23] Before the intracellular glucose detection, the uptake and localization of G-CSN into HepG2 cells were studied by 3D confocal fluorescence imaging. As shown in Figure 3 a–c, a strong red fluorescence signal was observed and well distributed throughout the entire cytoplasm of HepG2 cells, indicating the successful intracellular uptake of G-CSN. To demonstrate the intracellular glucose detection using G-CSN, HepG2 cells were pretreated with different concentrations of exogenous glucose and insulin before imaging because insulin can significantly increase intracellular glucose levels through the glucose transporter 4 (GLUT4) transporting process.[24] As expected, when treated with 1 mM glucose, G-CSN labeled cells showed a slightly stronger CL signal than those in the absence of glucose (Figure 3 d). Meanwhile, further enhanced CL signal was observed after incubation with a higher concentration of glucose (20 mM), demonstrating the effect of exogenous glucose on the intracellular glucose level. In addition, after the simultaneous pretreatment of glucose and insulin, a much stronger CL signal was observed in the cells. These results showed that insulin could promote the transport of glucose from the extracellular environment into the intracellular environment, indicating the important role of insulin in adjusting intracellular glucose levels.

The positive response of G-CSN-labelled cells towards insulin was also confirmed. As shown in Figure 4, HepG2 cells

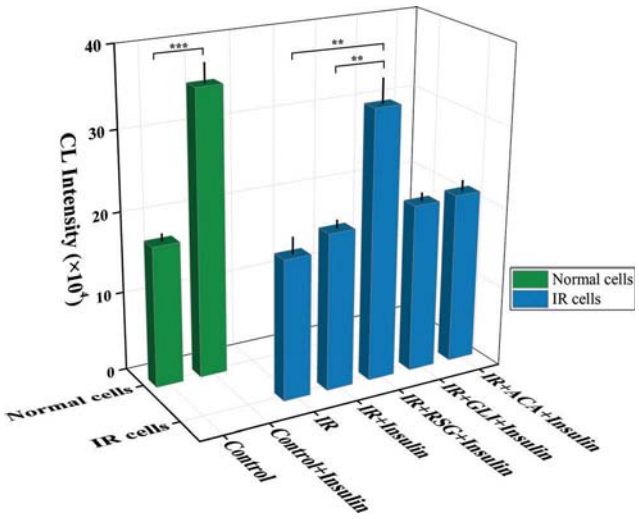

Figure 4. Response of G-CSN-labeled cells under various physiological conditions for insulin sensitizer screening. Statistical analysis was performed using independent-sample *t*-tests, *** $P < 0.001$, ** $P < 0.01$. All data represent mean ± SD ($n = 3$).

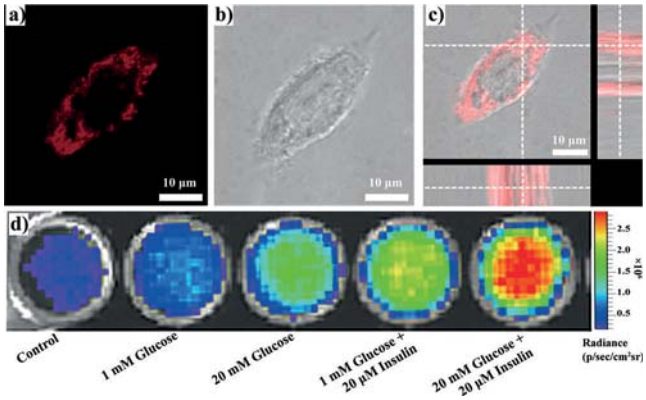

Figure 3. a–c) Laser scanning confocal microscopy (LSCM) images of HepG2 cells incubated with G-CSN for 30 min (RhB = Red): a) Fluorescence and b) bright-field images and c) overlay image: Z-projection (main), YZ-plane (right), XZ-plane (bottom). d) Luminescence images of G-CSN detection of intracellular glucose using after incubation of HepG2 cells for 30 min in the glucose-free culture media containing (from left to right) 0 mM glucose, 1 mM glucose, 20 mM glucose, 1 mM glucose and 20 μM insulin, and 20 mM glucose and 20 μM insulin. Before imaging, extracellular glucose and G-CSN were removed.

incubated in insulin exhibited a two-fold CL intensity increase over those in the control group, implying their higher intracellular glucose level induced by insulin. After a 48 h incubation with insulin, the cells did not show a significant further increase in glucose levels, which suggests that the long-term incubation of insulin could effectively transform the normal cells into insulin resistant (IR) cells. Based on this, insulin sensitizers could be screened by monitoring the intracellular glucose levels in IR HepG2 cells under exposure to various diabetic drugs. As a demonstration, rosiglitazone (RSG), an insulin sensitizers, was chosen as the positive medicine, and glibenclamide (GLI) and acarbose (ACA), two drugs used to treat diabetes through non-insulin-related mechanisms, were chosen as the negative medicines.[25] As expected, after treatment of IR cells with RSG and further stimulation with insulin, the level of intracellular glucose of IR HepG2 cells increased compared to that of IR cells without the RSG treatment. Moreover, this level was close to that of insulin-treated non-resistance cells, which indicated the recovery of the sensitivity of IR cells after exposure to RSG. However, the intracellular glucose level of negative groups did not show an obvious increase. To further verify that the intracellular luminescent emission is due to the GOx-

catalyzed generation of H_2O_2, an inhibitor of GOx, silver sulfate, was used. As expected, in the presence of silver sulfate, the CL was dramatically reduced compared with the group without silver sulfate, whether extracellular or intracellular (Supporting Information, Figure S10). These results suggested that G-CSN can be successfully used to screen insulin sensitizers.

In theory, the CSNs with H_2O_2-mediated PO-CL probes and oxidases could provide a general platform to detect any substrates that could be oxidized by corresponding oxidases and produce H_2O_2. These substrates include glucose, lactate, uric acid, ethanol, cholesterol, choline, L-lysine, fatty acids, pyruvate, glutamate, xanthine, D-galactose, amino acids, and *sn*-glycerol-3-phosphate. We explored the universality of the proposed oxidase-coated CSN for the detection of three other disease-diagnosis- or drunk-driving-related biomarkers (that is, lactate, uric acid, and ethanol). Similarly to the GOx adsorption, we coated PO-CL probes with lactate oxidase (L-CSN), uricase (U-CSN), and alcohol oxidase (A-CSN) to construct three types of biomarker probes. They were used to detect extracellular lactic acid (Supporting Information, Figures S11 and S12), uric acid (Supporting Information, Figures S13 and S14), and ethanol (Supporting Information, Figures S15 and S16), respectively. All the oxidase-incorporated CSNs exhibited linear response relationships between the CL intensities and the concentrations of their corresponding biomarkers. The limits of detection (LOD, 3σ) were 0.36, 0.31, and 0.37 μM for lactic acid, uric acid, and ethanol, respectively. These LODs were much lower than the concentration of the biomarkers in real biological samples, and lower than those of some fluorescent methods,[3c,d] showing the practical applicability in clinical diagnosis.

In conclusion, we presented a novel CSN for the intracellular profiling of oxidase-catalyzed biomarkers for disease diagnosis and screening of insulin sensitizers for drug development. As a demonstration, the representative biomarkers glucose, alcohol, L-lactic acid, and uric acid were successfully detected. Furthermore, insulin sensitizers were also accurately discriminated for diabetes treatment by using the G-CSN. Taking advantage of its sensitivity and specificity, this versatile oxidase-coated CSN system can serve as a useful platform for studying specific biomarkers in vitro and in vivo by a series of catalytic oxidation and CL reactions, even for monitoring biomarkers (such as acetyl choline and creatinine) that require multiple oxidases to produce H_2O_2. Therefore, the current approach showed potential applications in new drug development for insulin resistance and other disease-related biomarker monitoring (lactic acidosis and gout).

Acknowledgements

Financial support was provided by the National Natural Science Foundation of China (No. 21675016), Chongqing Basic and Frontier Research Program (No. cstc2016jcyjA0328), and the 100 Young Plan by Chongqing University (No. 0236011104410).

Conflict of interest

The authors declare no conflict of interest.

Keywords: biomarkers · chemiluminescence · insulin sensitizers · peroxisomes · silica nanodevices

How to cite: *Angew. Chem. Int. Ed.* **2017**, *56*, 14596–14601
Angew. Chem. **2017**, *129*, 14788–14793

[1] a) O. Veiseh, R. Langer, *Nature* **2015**, *524*, 39–40; b) R. A. Kreisberg, *Ann. Intern. Med.* **1980**, *92*, 227–237; c) K. L. Rock, H. Kataoka, J.-J. Lai, *Nat. Rev. Rheumatol.* **2013**, *9*, 13–23; d) D. E. Kelley, B. Goodpaster, R. R. Wing, J.-A. Simoneau, *Am. J. Physiol. Endocrinol. Metab.* **1999**, *277*, E1130–E1141; e) A. R. Saltiel, C. R. Kahn, *Nature* **2001**, *414*, 799–806.

[2] a) L. Denoroy, L. Zimmer, B. Renaud, S. Parrot, *J. Chromatogr. B* **2013**, *927*, 37–53; b) M. M. Khamis, D. J. Adamko, A. El-Aneed, *Mass Spectrom. Rev.* **2017**, *36*, 115–134; c) A. Chen, S. Chatterjee, *Chem. Soc. Rev.* **2013**, *42*, 5425–5438.

[3] a) X. Sun, W. Zhai, J. S. Fossey, T. D. James, *Chem. Commun.* **2016**, *52*, 3456–3469; b) J. C. Pickup, F. Hussain, N. D. Evans, O. J. Rolinski, D. J. S. Birch, *Biosens. Bioelectron.* **2005**, *20*, 2555–2565; c) N. E. Azmi, N. I. Ramli, J. Abdullah, M. A. Abdul Hamid, H. Sidek, S. Abd Rahman, N. Ariffin, N. A. Yusof, *Biosens. Bioelectron.* **2015**, *67*, 129–133; d) X. Shen, G. Zhang, D. Zhang, *Org. Lett.* **2012**, *14*, 1744–1747.

[4] H. Y. Lee, J. J. Lee, J. Park, S. B. Park, *Chem. Eur. J.* **2011**, *17*, 143–150.

[5] F. Leblond, S. C. Davis, P. A. Valdés, B. W. Pogue, *J. Photochem. Photobiol. B* **2010**, *98*, 77–94.

[6] a) L. L. Bronsart, C. Stokes, C. H. Contag, *Mol. Imaging Biol.* **2016**, *18*, 166–171; b) P. Li, L. Liu, H. Xiao, W. Zhang, L. Wang, B. Tang, *J. Am. Chem. Soc.* **2016**, *138*, 2893–2896; c) M. G. Azam, M. Yamasuji, T. Krawczyk, T. Shibata, T. Kabashima, M. Kai, *Talanta* **2015**, *139*, 138–142.

[7] a) M. Deng, S. Xu, F. Chen, *Anal. Methods* **2014**, *6*, 3117–3123; b) S. Wabaidur, S. Alam, Z. Alothman, G. Eldesoky, *Luminescence* **2014**, *29*, 684–688; c) J. Shu, Z. Qiu, Q. Zhou, Y. Lin, M. Lu, D. Tang, *Anal. Chem.* **2016**, *88*, 2958–2966.

[8] a) I. A. Smellie, J. K. D. Aldred, B. Bower, A. Cochrane, L. Macfarlane, H. B. McCarron, R. O'Hara, I. L. J. Patterson, M. I. Thomson, J. M. Walker, *J. Chem. Educ.* **2017**, *94*, 112–114; b) L. Yang, G. Guan, S. Wang, Z. Zhang, *J. Phys. Chem. C* **2012**, *116*, 3356–3362.

[9] M. M. Rauhut, L. J. Bollyky, B. G. Roberts, M. Loy, R. H. Whitman, A. V. Iannotta, A. M. Semsel, R. A. Clarke, *J. Am. Chem. Soc.* **1967**, *89*, 6515–6522.

[10] S. Cho, O. Hwang, I. Lee, G. Lee, D. Yoo, G. Khang, P. M. Kang, D. Lee, *Adv. Funct. Mater.* **2012**, *22*, 4038–4043.

[11] D. Lee, S. Khaja, J. C. Velasquez-Castano, M. Dasari, C. Sun, J. Petros, W. R. Taylor, N. Murthy, *Nat. Mater.* **2007**, *6*, 765–769.

[12] C. He, Y. Hu, L. Yin, C. Tang, C. Yin, *Biomaterials* **2010**, *31*, 3657–3666.

[13] L. A. Adutwum, N. Kishikawa, K. Ohyama, S. Harada, K. Nakashima, N. Kuroda, *Anal. Bioanal. Chem.* **2010**, *398*, 823–829.

[14] a) A. Singh, Y. H. Seo, C.-K. Lim, J. Koh, W.-D. Jang, I. C. Kwon, S. Kim, *ACS Nano* **2015**, *9*, 9906; b) C.-K. Lim, Y.-D. Lee, J. Na, J. M. Oh, S. Her, K. Kim, K. Choi, S. Kim, I. C. Kwon, *Adv. Funct. Mater.* **2010**, *20*, 2644–2648.

[15] M. Schrader, H. D. Fahimi, *Biochim. Biophys. Acta Mol. Cell Res.* **2006**, *1763*, 1755–1766.

[16] E. Katz, I. Willner, *Angew. Chem. Int. Ed.* **2004**, *43*, 6042–6108; *Angew. Chem.* **2004**, *116*, 6166–6235.

[17] J. M. Rosenholm, A. Meinander, E. Peuhu, R. Niemi, J. E. Eriksson, C. Sahlgren, M. Lindén, *ACS Nano* **2009**, *3*, 197 – 206.
[18] G. C. Van de Bittner, E. A. Dubikovskaya, C. R. Bertozzi, C. J. Chang, *Proc. Natl. Acad. Sci. USA* **2010**, *107*, 21316 – 21321.
[19] Y. Kim, G. Jang, D. Kim, J. Kim, T. S. Lee, *Polym. Chem.* **2016**, *7*, 1907 – 1912.
[20] J. Lu, M. Liong, J. I. Zink, F. Tamanoi, *Small* **2007**, *3*, 1341 – 1346.
[21] H. J. Hecht, H. M. Kalisz, J. Hendle, R. D. Schmid, D. Schomburg, *J. Mol. Biol.* **1993**, *229*, 153 – 172.
[22] a) K. u. Hasan, M. H. Asif, M. U. Hassan, M. O. Sandberg, O. Nur, M. Willander, S. Fagerholm, P. Strålfors, *Electrochim. Acta* **2015**, *174*, 574 – 580; b) M. H. Asif, B. Danielsson, M. Willander, *Sensors* **2015**, *15*, 11787 – 11804.
[23] a) E. D. Abel, O. Peroni, J. K. Kim, Y.-B. Kim, O. Boss, E. Hadro, T. Minnemann, G. I. Shulman, B. B. Kahn, *Nature* **2001**, *409*, 729 – 733; b) N. J. Bryant, R. Govers, D. E. James, *Nat. Rev. Mol. Cell Biol.* **2002**, *3*, 267 – 277.
[24] S. Huang, M. P. Czech, *Cell Metab.* **2007**, *5*, 237 – 252.
[25] M. C. Granberry, V. A. Fonseca, *Am. J. Cardiovasc. Drugs* **2005**, *5*, 201 – 209.

Manuscript received: August 30, 2017
Revised manuscript received: September 25, 2017
Accepted manuscript online: September 28, 2017
Version of record online: October 20, 2017

